Research Article | Vol. 26, No. 20 | 1 Oct 2018 | OPTICS EXPRESS 26317
Optics EXPRESS

Integration of stimulated Raman gain and stimulated Raman losses detection modes in a single nonlinear microscope

RAJEEV RANJAN,[1] ANNALISA D'ARCO,[1] MARIA ANTONIETTA FERRARA,[1] MAURIZIO INDOLFI,[1] MICHELE LAROBINA,[2] AND LUIGI SIRLETO[1,*]

[1]*National Research Council (CNR), Institute for Microelectronics and Microsystems, 80131 Napoli, Italy*
[2]*National Research Council (CNR), Institute of Biostructures and Bioimages, 80145 Napoli, Italy*
[*]*luigi.sirleto@cnr.it*

Abstract: This work addresses some key challenges in the fields of bio and nanophotonics by stimulated Raman microscopy. We present the design and the implementation of a femtosecond stimulated Raman scattering microscope, equipped with three femtosecond laser sources, which allows the coexistence of stimulated Raman gain (SRG) and stimulate Raman losses (SRL) detection modes in a single microscopy setup and to generate images of the same region in succession, without adding or removing components. In order to demonstrate the switching between the two detection modes, SRL and SRG images of polystyrene beads are acquired and the images quality are evaluated and compared.

1. Introduction

Nowadays, stimulated Raman scattering (SRS) spectroscopy and microscopy can be deal with a number of key challenges in nano and biophotonics. Concerning nanophotonics, a recent fascinating research field is nonlinear optics at nanoscale. Tailoring nonlinear optical properties of nanomaterials is both an applicative issue, especially relevant for the design of an efficient light source device, and a fundamental issue, since the understanding of the interplay between light and nanostructures is still incomplete. Concerning SRS, only pioneering works or preliminary results have been reported in the literature [1,2]. A fundamental aspect, for the development of this field, is the measurement of Raman gain of nanostructured materials at the wavelength of interest for telecommunications [3–5].

Concerning biophotonics, it is well known that label-free stimulated Raman scattering microscopy allows to image a variety of molecular species, targeting their intrinsic chemical bonds at the crowded cellular fingerprint region (<1800 cm^{-1}) or at the high frequency C-H (>2800 cm^{-1}) [6–11]. However, in SRS microscopy, the detection specificity is usually compromised. Because of the differentiable vibrational signatures are finite and many biomolecular species share the similar chemical bonds, it is not easy to distinguish a target biomolecule from the sea of the other related species inside cells. To achieve this goal, a general bio-orthogonal chemical imaging platform has, in recent times, emerged by coupling SRS microscopy with small and Raman-active vibrational probes (e.g., alkynes and stable isotopes), which exhibits sensitivity, specificity, and biocompatibility for imaging small biomolecules [12]. These vibrational probes are both spectroscopically and biochemically orthogonal to the endogenous molecules inside cells, thus they show Raman peaks in the cell-silent region where no other peaks from endogenous molecules are present [12–15].

In ref [16] Zhang et.al. demonstrated nonlinear vibrational bioimaging by detecting femtosecond pulse stimulated Raman losses. It is worth noting that a 12 times larger stimulated Raman losses signal by femtosecond pulse excitation than picosecond pulse was demonstrated. Therefore, taking into account the low sensitivity of Raman-active vibrational

#337854 https://doi.org/10.1364/OE.26.026317
Journal © 2018 Received 5 Jul 2018; revised 6 Aug 2018; accepted 9 Aug 2018; published 25 Sep 2018

Optics EXPRESS

probes, femtosecond stimulated Raman microscopy appears as an attractive and unavoidable perspective. In addition, in literature, based on this method, a number of interesting biological applications have been reported, extending in the silent region and encouraging the bio-orthogonal chemical imaging platform based on femtosecond SRS microscopy [17–24].

SRS is a two beam process and, for femtosecond applications, one of the most used and reliable laser combination is a Ti:Sa plus an optical parametric oscillator (OPO). Typical and widespread commercial OPO are IR-OPO (Infrared radiation-OPO), whose tunability range is 1000-1600 nm. The combination Ti:Sa plus IR-OPO, allowing to explore the wavelength window of interest for telecommunications, satisfies the requirement of nanophotonics application. On the contrary, concerning biophotonics, although they are tailored for multimodal imaging, in the case of SRS microscopy, they present a severe limitation: the minimum investigable Raman shift is 2500 cm^{-1}. Therefore, using Ti:Sa plus IR-OPO laser combination, only the CH region of Raman spectra can be explored, while the silent and fingerprint region are out of emission range [25,26]. As a consequence, the combination Ti:Sa plus IR-OPO cannot accomplish the demand of biorthogonal platform based on femtosecond stimulated Raman microscopy and its investigation and its diffusion has been in the past hopelessly compromised.

Recently, concerning widely tunable ultrafast laser system for multiphoton imaging, a new lasers combination has been commercialized, which presents a broad 680 nm to 1300 nm continuous, gap free tuning beam from a single source, equipped with a fixed beam at 1045 nm as dual beam option. This new laser source allows to investigate the C-H region (>2500 cm^{-1}), the silent region (1800-2800 cm^{-1}) and the fingerprint region (<1800 cm^{-1}), too, while rules out nanophotonics applications.

In this work, we present the design and the implementation of a femtosecond stimulated Raman scattering microscope, equipped with three femtosecond laser sources: a Ti:Sa, an IR-OPO and a second harmonic generator (SHG) optimized for the OPO. The proposed microscope has the merit to overcome the limitation of the two previous approach, i.e. to maintain the possibility to explore the window wavelength of interest for telecommunication and, in principle, to explore silent and finger print region, too, taking advantage of two possible laser combinations. The first, Ti:Sa and OPO, in stimulated Raman gain (SRG) detection mode, covers only the C-H region (>2800 cm^{-1}) but allows to investigate the window wavelength of interest for telecommunication. The second, Ti:Sa and SHG, covers not only the C-H region but also the silent region (1800-2800 cm^{-1}) and the fingerprint region (<1800 cm^{-1}), in stimulated Raman loss (SRL) detection mode.

Our approach provides a reasonable option in term of cost, because allows to avoid to buy two laser systems, which concerning tunability, present wavelengths ranges that are almost overlapped. The issue is the introduction of a third femtosecond source, which could make the performance of microscope worse. Therefore, in order to prove that our approach is reliable, SRL and SRG images of polystyrene beads using the two lasers combination are acquired and the images quality are evaluated and compared.

2. SRS microscope implementation

Our microscope, schematically reported in the Fig. 1, is obtained as a result of integration between a femtosecond-SRS (fs-SRS) spectroscopy setup and a microscope, which is made up by an inverted Nikon Ti-eclipse microscope and a scan head (C2 Nikon) equipped with 2D galvo mirrors. The microscope is equipped with three femtosecond laser sources. The first one, a femtosecond Ti:Sa (Chameleon Ultra II) with a pulse duration of approximately 140 fs, a repetition rate of 80 MHz and emission wavelengths in the range 680 - 1080 nm. The second one, a femtosecond synchronized infrared optical parametric oscillator (Chameleon Compact OPO), pumped by the Ti:Sa, with a pulse duration of approximately 200 fs, a repetition rate of 80 MHz and with range of emission wavelengths 1000 - 1600 nm. The third one, a frequency converter for ultrafast lasers, i.e. a second harmonic generation, cascading

Optics EXPRESS

the IR-OPO and doubling its energy radiation. In our experimental setup, the switching between the Ti:Sa-OPO and Ti:Sa-SHG lasers combinations is obtained by placed a flip mirror (FM) after the IR-OPO exit. When the mirror is inserted in optical path, IR-OPO radiation is coupled into SHG and Ti:Sa-SHG lasers combination becomes available, whereas when the mirror is flipped, the OPO can go on undisturbed and Ti:Sa – IR-OPO lasers combination becomes available.

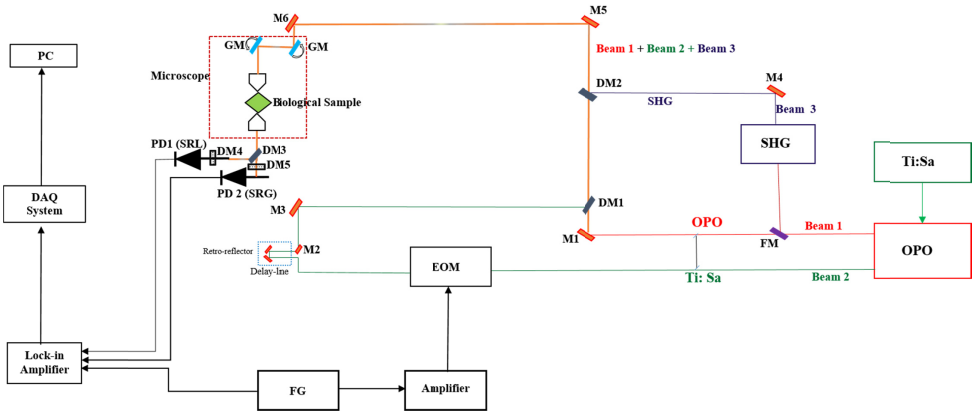

Fig. 1. Schematic layout of the f-SRS microscope. Ti:Sa = Titanium-Sapphire laser, OPO = Optical Parametric Oscillator, SHG = Second Harmonic Generator, M1 – M6 = Mirrors, FM = Flip Mirror, DM1, DM2, DM3 = dichroic mirrors, DM4, DM5 = notch filters, EOM = Electro-Optic Modulator, FG = Function Generator, GM = Galvo Mirror, PD1, PD2 = Photodiodes, DAQ = Data acquisition system, PC = Personal Computer.

The SHG is added in order to extend the SRS microscope capability. Pumping by Ti:Sa according to the excitation wavelength range (740 - 880 nm), the OPO emission range is into the range 1000 nm and 1600 nm, while the SHG emission range is into the range 500 - 800 nm. In Fig. 2, the Raman shift for Ti:Sa - SHG lasers sources combination as a function of entire Ti:Sa pumping wavelength range (740-880 nm) is reported. As an example, pumping by 810 nm wavelength, the OPO generates a wavelength into the range 1015 - 1536 nm and SHG emission wavelengths can be tuned into the narrow range: 645 - 765 nm. Therefore, the minimum and maximum Raman shift are given by 675 cm^{-1} and 3182 cm^{-1}, respectively (see red vertical line in Fig. 2). The largest range of Raman shift is obtained pumping OPO with 830 nm. In this case all the region of Raman spectra can be covered (from 451 cm^{-1}, to 3195 cm^{-1}), using the Ti:Sa - SHG lasers source combination (see black vertical line in Fig. 2). In addition, we note that in Fig. 2 the saffron and blue lines indicate minimum and maximum Raman shift, for Ti:Sa-SHG laser sources combination obtained pumping the OPO into the range [740-880] nm (we note that in Table 1, combinations of the pump wavelengths injection leading to generation of the second harmonic wavelengths are reported).

Optics EXPRESS

Table 1. Combinations of the pump wavelengths injection leading to generation of the second harmonic wavelengths

Ti:Sa	OPO (Min)	OPO (Max)	SHG (Min)	SHG(Max)	Raman Shift (Max)	Raman Shift (Min)
740	1000	1302	599	651	3180	1847
750	1000	1336	605	668	3195	1636
760	1000	1369	612	684	3181	1461
770	1000	1402	618	701	3194	1278
780	1000	1436	625	718	3179	1107
790	1000	1469	631	734	3189	965
800	1000	1502	637	751	3198	815
810	1015	1536	644	768	3182	675
820	1030	1569	650	784	3189	559
825	1038	1586	653	793	3192	489
830	1045	1602	656	800	3195	451
835	1053	1602	659	800	3198	523
840	1060	1602	663	800	3178	595
850	1075	1602	669	800	3182	735
860	1090	1602	675	800	3186	872
870	1105	1602	681	800	3190	1005
880	1120	1602	687	800	3192	1136

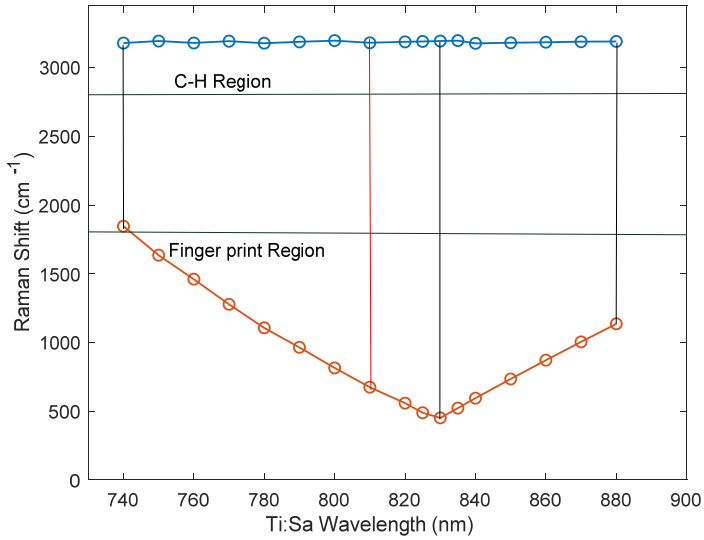

Fig. 2. Raman shift for Ti:Sa-SHG laser sources combination as a function of Ti:Sa pumping wavelengths. The vertical red line represents the range of Raman shift obtained pumping OPO by the Ti:Sa wavelength used in our experiment (810 nm). The vertical black line represents the largest range of Raman shift, which is obtained pumping OPO by the Ti:Sa wavelength of 830 nm. The saffron and blue lines indicate minimum and maximum Raman shift, for Ti:Sa-SHG laser sources combination obtained pumping the OPO into the range [740-880] nm.

In SRS microscopy, sensitive detection of the signal requires the implementation of a high-frequency modulation transfer scheme. By modulating one of the beams at a known frequency with an electro-optic modulator (EOM) and measuring the modulation transfer to the originally unmodulated beam at the same frequency, SRS can be detected specifically [25]. If the modulation frequency is faster than the typical laser noise (e.g. 1 MHz), high sensitivity detection is achieved at the moderate laser power required for biological and medical imaging. In SRS microscope implementation, EOM plays an important role, since it affects cost of system, covers space on the optical bench and produces unwanted electromagnetic interference. In our SRS microscope design, even if three laser sources are

Optics EXPRESS

used, the use of a single EOM with a fixed position on the bench is desirable, in order to save time and increase flexibility of our setup. We note that the choice of laser source modulated by EOM has relevant consequences, because it defines the modalities SRL or SRG that can be utilized. In our setup the EOM (350-160 KD*P CONOPTICS) is used for Ti:Sa pulses intensity modulation at a frequency *f* in the range of 1-30 MHz. Therefore, for the Ti:Sa and OPO combination, the modulated laser beam is always greater than the other one, this means that a SRG scheme must be implemented, whereas, for the Ti:Sa-SHG combination, the modulated laser beam is always lower than the other one, so that a SRL scheme can be implemented. In Fig. 3 the two possible combinations of laser sources (Ti:Sa-OPO and Ti:Sa-OPO + SHG) along with their measurement modalities and their working ranges are reported.

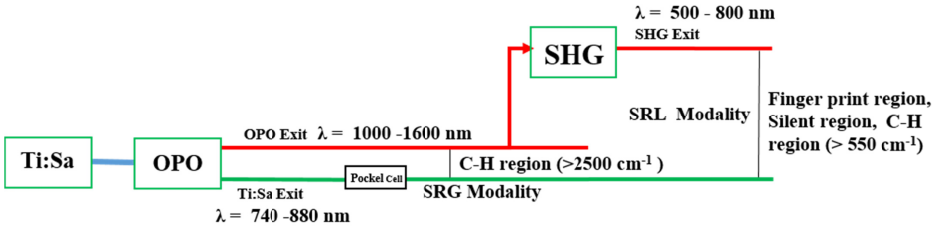

Fig. 3. Generation system with combination of. Ti:Sa, OPO and SHG.

In order to generate a SRS signal, the pump and probe pulsed lasers must be overlapped in both space and time at the image plane. OPO technology have allowed perfect synchronization between Ti:Sa and OPO beams. However, since these two beams inside the OPO housing follow slightly different beam paths, to ensure temporal overlap at the sample, a precise tunable optical delay has to be utilized. In our case, at the OPO exit, Ti:Sa and OPO beams have a time delay of about 5 ns and they were temporally overlapped by a delay line (Newport MOD M-ILS200CC) inserted between the Ti:Sa and the microscope. Concerning Ti:Sa - SHG lasers combination, we note that the propagation inside SHG does not change significantly the delay time with respect to OPO, but introduces an additional optical path with respect to Ti:Sa. Therefore, when we want to select the combination Ti:Sa - SHG, temporal overlap between Ti:Sa and SHG is achieved by a fixed shift movement of delay line with respect to the Ti:Sa - OPO overlap position. In order to reduce cost and to save space, the use of a single delay line is desirable and to achieve coexistence between SRL and SRG optical circuitries, its position on the bench has to be fixed. Our microscopic system has flexible designed, so that if we want to switch between the two possible combinations of laser beams, the temporal overlap of each combination is achieved by using a single delay line with a fixed position on the bench and only by changing the direction of a delay line fixed shift movement. Ti:Sa and OPO beams were spatially collinearly combined by a dichroic mirror (DM1; Semrock FF875-Di0125x36), which transmits OPO and reflects Ti:Sa, while, Ti:Sa-SHG beams were spatially collinearly combined by a dichroic mirror (DM2; Semrock FF875-Di0125x36), which is placed after DM1. We note that being DM2 a high bandpass filter, whose transparence band start to 735 nm, any wavelengths selected by Ti:Sa - OPO lasers combination is transmitted. Therefore, SRG optical circuitry, based on Ti:Sa - OPO combination is not influenced by DM2.

Another important requirement is the use of a sole microscope for both optical circuits. In our setup, both lasers combinations can be focused onto a focal spot inside a sample through a scanning unit by a 60X multiphoton microscope objective (Nikon, Plan Apo IR, NA 1.27). Output pulses are collected by a 40X high numerical aperture objective (Nikon, Apo 40X, NA 1.25). This is crucial for SRS techniques, where photo-thermal and position-dependent interference effects may introduce artifacts in the image [26,27], which can be reduced by choosing a high numerical aperture (NA) objectives.

Optics EXPRESS

Afterwards, the collected radiation is incident onto a high bandpass filter (Dichroic mirrorr FF875-Di01-25x36), whose transmission band start at 875 nm, introducing two perpendicular optical paths. The longitudinal one transmits OPO, while the perpendicular one reflects both Ti:Sa and SHG. Both paths are used to detect the unmodulated pulses (SHG beam for SRL modality and OPO beam for SRG modality) by two photodiodes (PD1, PD2) placed to the end of each path. In order to remove Ti:Sa modulated beam (pump pulses in SRG configuration and Stokes pulses in SRL configuration), DM4 and DM5 i.e. two notch filters (NF03-808E-25) placed in front of PD1, PD2, respectively, are used. To optimize the acquisition efficiency, a Thorlabs detector (PD1; DET10A/M, Si Detector) for SRL measurements and a Thorlabs detector (PD2; DET10N/M, InGaAs Detector) for SRG measurements are, respectively, used. Finally, photodiode readout is demodulated by a lock-in amplifier (LIA) (SR844- 200 MHz dual phase) to extract the modulation depth at the frequency *f*. In order to collect information and to obtain a 2D image, the electrical signal coming out from the LIA is digitalized by PCI card (NI PCIe 6363), which manages and synchronizes the lock-in amplifier and the scanning unit of microscope by an in-house developed LabVIEW program.

3. Results and discussion

Since one of the aim of the paper is to perform a measurement of the image quality, all the images are raw ones, single recordings of 255 px × 255 px, with an acquisition times of 16 s.

In the Fig. 4, on the left, Fig. 4(a), SRL image with a scanning zoom of 2x, while on the right, Fig. 4(b), SRG image with a scanning zoom of 3.5x of a polystyrene beads sample are, respectively, reported. They were obtained recording polystyrene beads with a diameter of 3 μm, by matching the Raman shift at 3054 cm^{-1}, associated with CH bond. For SRG images, the pump signal generated by Ti:Sa was set to 810 nm, while the probe signal generated by OPO was set at 1076 nm, for both of them the average focused power was about 10 mW. For SRL imaging, the pump signal generated by SHG unit was set at 650 nm, while the probe signal was still at 810 nm. The average focused power for Ti:Sa and SHG were 8 mW and 6 mW, respectively.

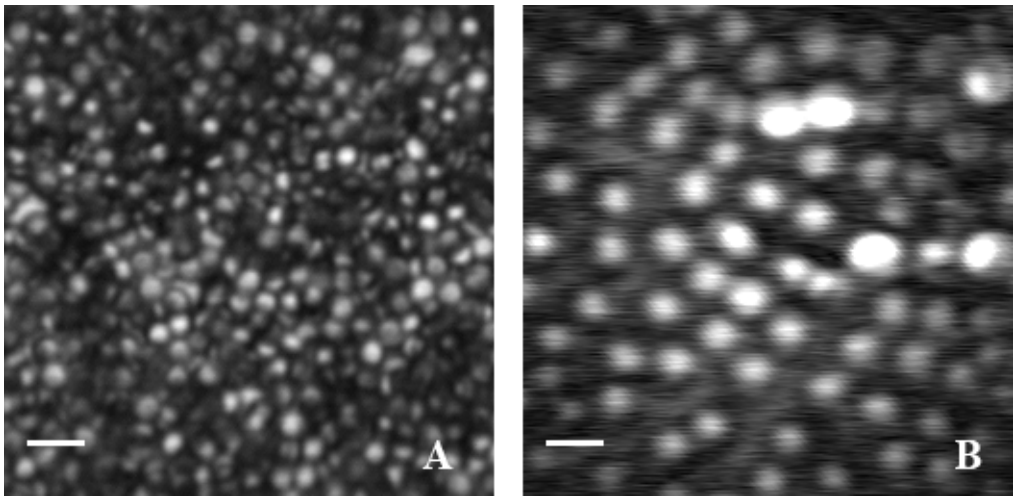

Fig. 4. Images of polystyrene beads taken from f-SRS microscope at 3054 cm^{-1}. A) SRL image, scale bar: 6 μm; B) SRG image, scale bar: 3.5 μm.

We note that for both images, the samples were prepared depositing a drop of solution, containing beads with the same dimensions (3 μm), onto cover glass without flattening it, and placing the second cover glass after drying. However, due to the bigger zoom used in SRG acquisition, in Figs. 4(b) the optical section capability of SRS is better highlighted, i.e. the

Optics EXPRESS

sectioning of beads placed on different planes, locating circles of different radius, is more evident.

For the evaluation of image quality, we used the signal-to-noise ratio (SNR) parameter, which was calculated as the ratio of the mean signal value of the imaged object (Mean(object)) to the standard deviation of the background (SD(background)) [28-30].

$$\mathbf{SNR} = \frac{\text{Mean(object)}}{\text{SD(background)}} \quad (1)$$

In order to estimate the SNR, it was necessary to separate in the image the background from the foreground (see Fig. 5). Starting from an initial estimate that assume the fraction of foreground pixels to be the 50%, background image was generated considering all the pixels of the image with intensities value less than a threshold value I_{th1}. This value was manually individuated using the ImageJ 'adjust threshold' function, taking into account the histogram of image. Using this background image, the Mean and the SD of the background were calculated. In a similar way, a foreground image was generated considering all the pixels of the image with intensities value greater than a threshold value I_{th2}. This value was manually individuated using the ImageJ 'adjust threshold' function selecting pixels clearly representing the imaged object. The obtained foreground image was used to calculate the Mean and the SD of the imaged object. Schematic of the evaluation process is reported in Fig. 5.

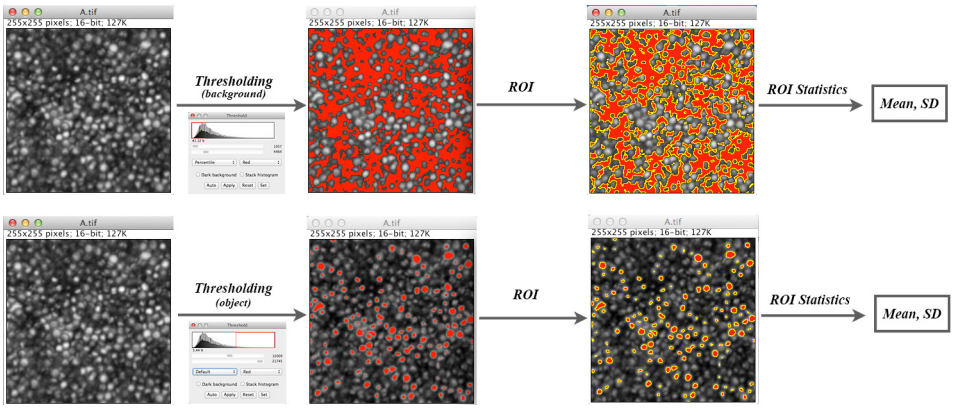

Fig. 5. Schematic of the evaluation process.

In order to test reliability of our procedure, the SNR was estimated by the Deconvolution Express function of the Huygens software v. 17.04 (Scientific Volume Imaging) and how reported in Table 2 there is no a significant different between the values obtained with the two methods. We note that SRS microscopes based on femtosecond laser sources are not commercial systems. Therefore, there are no metric or references that can be used to put our number in perspectives. However, as a general criterion for commercial systems based on other types of contrast, for a detectable signal, the SNR values must be at least higher than 5 [31].

Table 2. The estimated SNR values provided by the Deconvolution Express function of the Huygens software v. 17.04 (Scientific Volume Imaging) and by our in-house software are reported for comparison.

Acquisition Modality	SNR	
	Calculated value	Huygens Software
SRG	23.1	26.0
SRL	27.0	25.0

Optics EXPRESS

In our system in order to ensure flexibility and to reduce cost and space taken up the optical bench, a single electro-optic modulator, a single delay line and a single optical microscope are shared by both SRG and SRL modalities. In addition, in order to switch between the two detection modes, we have only to move the delay line at a fixed position and to flip the mirror. However, in next future, in order to improve reproducibility and to run the two detection mode simultaneously, we have two options. The first, we plan to add a second delay line in SHG or OPO signal paths, which can fix the delay time between Ti:Sa and SHG beams. The second, we plan to substitute the flip mirror with an infrared nonpolarizing beam splitter. Now this replacement is feasible, because we are sure that the values of power needed for exciting SRS are enough also if we divide at 50% the exit of OPO.

In near future we are going to investigate the C-H region and the silent region, for some specific biological applications. Taking advantage of our proposed microscope, we note that both SRG and SRL detection modes allow the C-H region investigation. However, SRG detection mode is advisable, because infared wavelength can be used, while for SRL detection mode visible wavelength should be used and thermal effects could influence the measurements. For the silent region, using our microscope, SRL modalities is the only option, and the required wavelengths are into near infrared range (720-810 nm). It is worth noting that in order to carry out measurements in the silent region, we have only to set suitable Ti:Sa and SHG wavelengths (for example for silent region), therefore the system is ready for use.

Before concluding, we note that our approach has the merit to overcome the limits of both approach Ti:Sa plus IR-OPO and, recently commercialized, widely tunable ultrafast laser system for multiphoton imaging. It takes advantage of extended range of IR-OPO approach useful for nanophotonics applications, and has the potentiality, in principle, to extend the working range of SRS microscope based on Ti:Sa and IR-OPO in fingerprint and in silent regions, which is an important perspectives for bio-orthogonal chemical imaging platform. In addition, we note that spectral focusing, which is one of the most promising techniques for hyperspectral imaging could be implemented in our system, without obstacles [32,33].

4. Conclusions

In conclusions, in this paper, the implementation of a femtosecond stimulated Raman microscope, using three femtosecond laser sources, is reported, allowing the coexistence of stimulated Raman gain and stimulate Raman losses detection mode in a single microscopy setup. In order to demonstrate the successful realization of f-SRS microscope, the Raman shift at 3054 cm^{-1}, associated with CH bond, has been investigated in polystyrene beads sample. Evaluated signal-to-noise ratio (SNR) prove that SRG and SRL modalities yield comparable images quality, thus demonstrating that the use of a third laser source does not induce a deterioration in the performance of our imaging system.

Funding

Italian National Operative Programs PONa3_00025 (BIOforIU) and by Euro-bioimaging large scale pan-European research infrastructure project.

Acknowledgments

The authors would like to thank Dr. Giacomo Cozzi, a product specialist from Nikon Instruments, for his support in the SRS microscopy implementation; Vitaliano Tufano (IMM-CNR) for his precious and constant technical assistance.

References

1. L. Sirleto, M. A. Ferrara, T. Nikitin, S. Novikov, and L. Khriachtchev, "Giant Raman gain in silicon nanocrystals," Nat. Commun. **3**(1), 1220 (2012).
2. L. Sirleto, A. Vergara, and M. A. Ferrara, "Advances in stimulated Raman scattering in nanostructures," Adv. Opt. Photonics **9**(1), 169 (2017).
3. L. Sirleto, M. A. Ferrara, I. Rendina, S. N. Basu, J. Warga, R. Li, and L. Dal Negro, "Enhanced stimulated

Optics EXPRESS

Raman scattering in silicon nanocrystals embedded in silicon-rich nitride/silicon superlattice structures," Appl. Phys. Lett. **93**(25), 251104 (2008).
4. L. Sirleto, M. A. Ferrara, G. Nicotra, C. Spinella, and I. Rendina, "Observation of stimulated Raman scattering in silicon nanocomposites," Appl. Phys. Lett. **94**(22), 221106 (2009).
5. L. Sirleto, M. A. Ferrara, and A. Vergara, "Toward an ideal nanomaterial for on-chip Raman laser," J. Nonlinear Opt. Phys. Mater. **26**(03), 1750039 (2017).
6. W. Min, C. W. Freudiger, S. Lu, and X. S. Xie, "Coherent Nonlinear Optical Imaging: Beyond Fluorescence Microscopy," Annu. Rev. Phys. Chem. **62**(1), 507–530 (2011).
7. D. Zhang, P. Wang, M. N. Slipchenko, and J.-X. Cheng, "Fast Vibrational Imaging of Single Cells and Tissues by Stimulated Raman Scattering Microscopy," Acc. Chem. Res. **47**(8), 2282–2290 (2014).
8. J.-X. Cheng and X. S. Xie, "Vibrational spectroscopic imaging of living systems: An emerging platform for biology and medicine," Science **350**(6264), aaa8870 (2015).
9. C. H. Camp, Jr. and M. T. Cicerone, "Chemically sensitive bioimaging with coherent Raman scattering," Nat. Photonics **9**(5), 295–305 (2015).
10. A. Alfonso-García, R. Mittal, E. S. Lee, and E. O. Potma, "Biological imaging with coherent Raman scattering microscopy: a tutorial," J. Biomed. Opt. **19**(7), 071407 (2014).
11. A. Zumbusch, W. Langbein, and P. Borri, "Nonlinear vibrational microscopy applied to lipid biology," Prog. Lipid Res. **52**(4), 615–632 (2013).
12. L. Wei, F. Hu, Z. Chen, Y. Shen, L. Zhang, and W. Min, "Live-Cell Bioorthogonal Chemical Imaging: Stimulated Raman Scattering Microscopy of Vibrational Probes," Acc. Chem. Res. **49**(8), 1494–1502 (2016).
13. F. Hu, M. R. Lamprecht, L. Wei, B. Morrison, and W. Min, "Bioorthogonal chemical imaging of metabolic activities in live mammalian hippocampal tissues with stimulated Raman scattering," Sci. Rep. **6**(1), 39660 (2016).
14. L. Wei, F. Hu, Y. Shen, Z. Chen, Y. Yu, C. C. Lin, M. C. Wang, and W. Min, "Live-cell imaging of alkyne-tagged small biomolecules by stimulated Raman scattering," Nat. Methods **11**(4), 410–412 (2014).
15. L. Wei, Y. Shen, F. Xu, F. Hu, J. K. Harrington, K. L. Targoff, and W. Min, "Imaging complex protein metabolism in live organisms by stimulated Raman scattering microscopy with isotope labeling," ACS Chem. Biol. **10**(3), 901–908 (2015).
16. D. Zhang, M. N. Slipchenko, and J. X. Cheng, "Highly sensitive vibrational imaging by femtosecond pulse stimulated raman loss," J. Phys. Chem. Lett. **2**(11), 1248–1253 (2011).
17. Y. Ozeki, F. Dake, S. Kajiyama, K. Fukui, and K. Itoh, "Analysis and experimental assessment of the sensitivity of stimulated Raman scattering microscopy," Opt. Express **17**(5), 3651–3658 (2009).
18. C. Zhang, J. Li, L. Lan, and J. X. Cheng, "Quantification of Lipid Metabolism in Living Cells through the Dynamics of Lipid Droplets Measured by Stimulated Raman Scattering Imaging," Anal. Chem. **89**(8), 4502–4507 (2017).
19. W. Dou, D. Zhang, Y. Jung, J.-X. Cheng, and D. M. Umulis, "Label-Free Imaging of Lipid-Droplet Intracellular Motion in Early Drosophila Embryos Using Femtosecond-Stimulated Raman Loss Microscopy," Biophys. J. **102**(7), 1666–1675 (2012).
20. C. Zhang, K.-C. Huang, B. Rajwa, J. Li, S. Yang, H. Lin, C. Liao, G. Eakins, S. Kuang, V. Patsekin, J. P. Robinson, and J.-X. Cheng, "Stimulated Raman scattering flow cytometry for label-free single-particle analysis," Optica **4**(1), 103 (2017).
21. H. J. Lee, W. Zhang, D. Zhang, Y. Yang, B. Liu, E. L. Barker, K. K. Buhman, L. V. Slipchenko, M. Dai, and J.-X. Cheng, "Assessing Cholesterol Storage in Live Cells and C. elegans by Stimulated Raman Scattering Imaging of Phenyl-Diyne Cholesterol," Sci. Rep. **5**(1), 7930 (2015).
22. J. Li and J.-X. Cheng, "Direct Visualization of De novo Lipogenesis in Single Living Cells," Sci. Rep. **4**(1), 6807 (2015).
23. C.-R. Hu, D. Zhang, M. N. Slipchenko, J.-X. Cheng, and B. Hu, "Label-free real-time imaging of myelination in the Xenopus laevis tadpole by in vivo stimulated Raman scattering microscopy," J. Biomed. Opt. **19**(8), 086005 (2014).
24. A. D'Arco, N. Brancati, M. A. Ferrara, M. Indolfi, M. Frucci, and L. Sirleto, "Subcellular chemical and morphological analysis by stimulated Raman scattering microscopy and image analysis techniques," Biomed. Opt. Express **7**(5), 1853–1864 (2016).
25. A. D'Arco, M. A. Ferrara, M. Indolfi, V. Tufano, and L. Sirleto, "Label-free imaging of small lipid droplets by femtosecond-stimulated Raman scattering microscopy," J. Nonlinear Opt. Phys. Mater. **26**(04), 1750052 (2017).
26. K. I. Popov, A. F. Pegoraro, A. Stolow, and L. Ramunno, "Image formation in CARS and SRS: effect of an inhomogeneous nonresonant background medium," Opt. Lett. **37**(4), 473–475 (2012).
27. C.-Y. Chung, J. Hsu, S. Mukamel, and E. O. Potma, "Controlling stimulated coherent spectroscopy and microscopy by a position-dependent phase," Phys. Rev. A **87**(3), 033833 (2013).
28. M. A. Flower, *Webb's Physics of Medical Imaging* (Taylor & Francis, 2012).
29. S. E. and T. V. S. Jayaram, *Digital Image Processing* (Prentice Hall, 2009).
30. J. M. Mateos, and P. J. Broeke, *Image Processing with ImageJ*, 2nd ed. (Packt Publishing, 2015).
31. A. Rose, *Vision: Human and Electronic*, (New York: Plenum Press, 1973); pp. 21–23.
32. T. Hellerer, A. M. K. Enejder, and A. Zumbusch, "Spectral focusing: High spectral resolution spectroscopy with broad-bandwidth laser pulses," Appl. Phys. Lett. **85**(1), 25–27 (2004).
33. I. Rocha-Mendoza, W. Langbein, and P. Borri, "Coherent anti-Stokes Raman microspectroscopy using spectral

Optics EXPRESS

focusing with glass dispersion," Appl. Phys. Lett. **93**(20), 201103 (2008).